Journal of Nuclear Materials 408 (2011) 272–284

Contents lists available at ScienceDirect

Journal of Nuclear Materials

journal homepage: www.elsevier.com/locate/jnucmat

Interaction of carbon with vacancy and self-interstitial atom clusters in α-iron studied using metallic–covalent interatomic potential

Dmitry Terentyev [a,*], Napoleón Anento [b], Anna Serra [b], Ville Jansson [a,c], Hassan Khater [b], Giovanni Bonny [a]

[a] SCK-CEN, Nuclear Materials Science Institute, Boeretang 200, B-2400 Mol, Belgium
[b] Department Matemàtica Aplicada III, E.T.S. Enginyeria de Camins, Universitat Politècnica de Catalunya, Jordi Girona 1-3, 08034 Barcelona, Spain
[c] Department of Physics, University of Helsinki, P.O. Box 43, FI-00014, Helsinki 00014, Finland

ARTICLE INFO

Article history:
Received 16 July 2010
Accepted 25 November 2010
Available online 1 December 2010

ABSTRACT

The presence of even small amount of carbon interstitial impurity affects properties of Fe and Fe-based ferritic alloys. From earlier experiments it follows that carbon exhibits considerably strong interaction with lattice defects and therefore influences their mobility, hence affecting the evolution of the microstructure under irradiation. This work is dedicated to understanding the interaction of carbon–vacancy complexes with glissile dislocation loops, which form in Fe, Fe-based alloys and ferritic steels under irradiation. We apply large scale atomistic simulations coupled with the so-called 'metallic–covalent bonding' interatomic model for the Fe–C system, known to be the most consistent interatomic model available today. With these techniques we have studied (i) the stability of vacancy–carbon clusters; (ii) the interaction of octahedral carbon with ½⟨1 1 1⟩ loops; (iii) possibility of the dynamic drag of carbon by ½⟨1 1 1⟩ loops and (iv) the interaction of ½⟨1 1 1⟩ loops with the most stable vacancy–carbon clusters expected to occur under irradiation. Finally, we have shown that carbon–vacancy complexes act as strong traps for ½⟨1 1 1⟩ loops.

1. Introduction

Molecular dynamics (MD) simulations of displacement collision cascades in FCC and BCC metals suggest that clusters of self-interstitial atoms (SIA) are directly formed in collision cascades (see e.g. [1–3]). In most of the BCC transition metals the most favourable configuration of an isolated SIA is a ⟨1 1 1⟩ crowdion [4]. While in BCC Iron, it is a ⟨1 1 0⟩ dumbbell whose formation is by 0.7 eV lower than that of a ⟨1 1 1⟩ crowdion [5]. As a consequence of that, small SIA clusters form a platelet of ⟨1 1 0⟩ dumbbells, whereas larger clusters (with size above 6 SIAs) form a platelet of ⟨1 1 1⟩ crowdions [6]. So that, relatively large SIA clusters can already be described as ½⟨1 1 1⟩ dislocation loops [7]. These large clusters (or dislocation loops) can migrate from the cascade region by performing one dimensional motion with an extremely low activation energy (0.05 eV) [7,8]. In contrast, the migration of single vacancies, SIAs and their small clusters (with size up to ~5), proceeds via a three dimensional random walk [6,9]. The difference in the migration mechanisms between small and large SIA clusters is believed to affect kinetics and defect evolution depending on the source of irradiation (i.e. Frenkel pairs or cascade productive) and temperature [10–12]. Therefore, the study of 1D migration of SIA clusters in Fe and Fe–C solid solution is an important issue for the understanding of the accumulation of radiation damage in nominally pure Fe as well as in the Fe-based steels.

There are only few experimental methods allowing to detect 1D movement of SIA clusters and nano-metric dislocation loops. Recent transmission electron microscopy (TEM) studies discovered fast back and forth motion of interstitial clusters along close packed directions in Fe and its alloys [13–15]. This is consistent with the results of MD simulations [7,16,17]. However, there is an essential discrepancy between simulations and experiment in terms of the type of movement. Experimentally, 1D migration has been observed as discrete 1D jumps interrupted from time to time due to some invisible obstacles or traps at room temperature [14]. MD simulations predict a fast and continuous 1D random walk in pure bcc Fe even at temperatures below 100 K. The recently proposed Langevin model by Dudarev et al. suggests that the in situ experimental results can be explained taking into account the long range interaction between dislocation loops as well as their pinning on some invisible obstacles [18]. Small vacancy clusters, created due to ion irradiation, were suggested as possible traps. An interaction energy of 0.8 eV was shown to be enough to reproduce the experimentally observed profile of the loop migration at 675 K. We note, however, that this experimental temperature is well above stage V (~520 K), at which small vacancy clusters actively dissolve in pure Fe [19]. Hence, the

* Corresponding author. Tel.: +32 14 333197; fax: +32 14 321216.
E-mail address: dterenty@sckcen.be (D. Terentyev).

0022-3115/$ - see front matter © 2010 Elsevier B.V. All rights reserved.
doi:10.1016/j.jnucmat.2010.11.053

hypothesis of trapping on small vacancy clusters does not explain the experimental results obtained at high temperature.

In this work, we address the problem of the SIA cluster's trapping mechanism that may lead to the slowing down or complete blockage of highly mobile small (few tens of defects) ⟨1 1 1⟩ SIA clusters in bcc Fe. Beside the above mentioned experimental evidence, the need for the understanding of trapping is underlined by a number of recent computational studies on the evolution of the microstructure driven by electron, ion and neutron irradiation in pure Fe and Fe-based materials [9,20–22]. The latter studies were employing object kinetic Monte-Carlo simulations to address the accumulation of clusters of point defects. It was concluded that in order to obtain a reasonable agreement with experiment one needs either to postulate immobility of SIA clusters (starting from very small sizes) or to introduce traps for 1D mobile SIA clusters. Assuming that all loops are immobile, one contradicts the well established in situ TEM observations of the hopping of even relatively large SIA clusters. Therefore, residual impurities (such as carbon) were proposed to be a possible source of trapping and the dissociation energy was estimated by fitting the simulation results to experimental data to be ~1 eV. The trapping mechanism is not known experimentally because a typical size of the dislocation loops created directly in collision cascades is from few up to few tens of SIAs. Such defects are hardly resolvable by TEM techniques and, in addition, their high velocity (relying on MD studies) would not allow for the registration of the continuous movement due to the limit of the resolution of the best up-to-date existing CCD cameras. This is why TEM data, where abrupt movement of small SIA loops is observed, cannot be used directly to reveal the origin of the trapping.

2. Background

Atomistic simulations, employing semi-empirical interatomic potentials, so far revealed a binding energy of about 0.4–0.66 eV between an isolated carbon atom (hence forth C) in octahedral position and ⟨1 1 1⟩ SIA clusters (with size varying from 7 up to 19 SIAs) [23]. In the same work, the long range transport of C together with the loop was found not to be possible. The dissociation energy of an SIA cluster from C (henceforth E_D(L–C)) can be estimated as the sum of the binding energy and migration energy of an SIA cluster and C, which are 0.4–0.66 eV and 0.05 eV, respectively. This is considerably lower than the value of the trapping energy (1 eV) suggested in [20]. One may speculate that in-cascade created SIA clusters can be trapped by a few (or at least two) carbon atoms, which would provide the necessary trapping energy to explain the origin of trapping. However, such a multiple trapping requires the interaction with a second C atom when the C-cluster complex is immobile or the cluster is dragging the carbon atom. The former event should occur within a time characterized by the dissociation energy for a single carbon i.e. $\sim\exp(E_D(\text{L–C})/k_BT)/\nu_D$ (here k_B and ν_D are the Boltzmann's constant and the Debye frequency, respectively). Under irradiation the majority of carbon atoms in solution are expected to be in stable vacancy–carbon complexes such as v–C, v–C_2, and v_2–C, whose dissociation energy, obtained using *ab initio* calculations, is above 1 eV [24,25]. Thus, the dissociation time of such complexes exceeds the time during which an SIA cluster can be immobilized by a single carbon atom. Hence, the multiple trapping will occur upon the condition that the drag of C by SIA clusters is possible.

If C could actually be dragged by a ⟨1 1 1⟩ SIA cluster and the migration energy for the carbon moving together with the loop (henceforth E_M(L–C)) is considerably lower than E_D(L–C), the multiple carbon trapping would become rather probable. Thus, the migration of Carbon attached to the SIA and its binding energy are the key parameters deciding the mechanism responsible for the reduction of the mobility of 1D-glissile SIA clusters.

In addition to the pinning of SIA clusters by freely migrating carbon atoms, the blockage of 1D migrating clusters by stable and immobile v–C complexes should be considered. Up to our best knowledge, this mechanism has so far not been studied. Partially, the problem was the absence of a reliable Fe–C potential that provides a proper description for the C–C and C–V interaction in the Fe bulk. A direct application of density functional theory (DFT) calculations is prohibited when large SIA clusters are considered, whereas the reliability of the interatomic potential used in [23] with respect to the SIA–C interaction is doubtful. Indeed, the pairwise Johnson potential (henceforth *J*) [23,26] provides a strong attractive interaction of C in the immediate vicinity of a ⟨1 1 0⟩ dumbbell, which contradicts DFT data that predicts repulsive interaction. (A weak binding energy, 0.1 eV, between C and a ⟨1 1 0⟩ dumbbell was found only if the carbon is placed in the tensile region of the strain field of the dumbbell, see Ref. [27] for discussion.) The interatomic potential fails to reproduce DFT data because of the absence of the saturation of covalent bonding, as was revealed by DFT calculations. Thus, the interaction of SIA clusters with C should be essentially reconsidered. Recently, a new N-body EAM potential for the Fe–C system was suggested in [27]. The obtained potential essentially removes the shortcoming of the previously developed ones and provides a correct (i.e. in line with DFT data) trend for the energetics of v–C (covalent directional bonding), C – ⟨1 1 0⟩ SIA and C–C complexes in Fe matrix.

In this work we apply the newly developed potential to investigate: (i) the possibility for the drag of C by glissile ⟨1 1 1⟩ SIA clusters; (ii) the effect of C on the stability of small vacancy clusters (henceforth v–C complexes) and (iii) the interaction of ⟨1 1 1⟩ SIA clusters (or ½⟨1 1 1⟩ interstitial dislocation loop) with v–C complexes, namely: v–C, v_2–C and v–C_2. The latter issue was studied using the so-called 'loop-drag' model [28], where a ½⟨1 1 1⟩{1 1 0} edge dislocation is introduced in a system containing a loop with the same Burgers vector. An external shear stress is applied to induce dislocation movement. The dislocation, in turn, pulls/drags (depending on the interaction geometry) the loop. In this way, we accelerate or even provoke the interaction of the dislocation loop with a specific defect placed on the way of the gliding loop. In parallel we also address the problem of the interaction of carbon with small non-parallel SIA clusters reported in a recent study [29], to clarify whether carbon can further stabilize these structures.

The paper is organized as follows. In Section 3 we describe the computational details of the performed MS and MD simulations and features of the interatomic potentials used. Results are presented in Section 4, which is divided in two subsections describing data obtained using MS and MD techniques, respectively. A critical discussion and implications of the obtained results are presented in Section 5, and conclusions are drawn in Section 6.

3. Computational details

3.1. Important features of the applied interatomic potentials

To carry out the present study, we employ an Embedded Atom Method-type interatomic potential derived by Hepburn and Ackland (henceforth referred to as '*H*') [27]. The so-called 'metallic–covalent bonding' potential was specifically developed to fix long standing problems related to the description of: (i) carbon–carbon interaction in bulk bcc Fe; (ii) the interaction of carbon with over-coordinated defects (i.e. self-interstitial atoms); and (iii) the energetics of carbon–vacancy complexes (such as C_2–v and v_2–C). As a benchmark we also apply two other interatomic potentials, extensively used to characterize the effect of Carbon on the stability of

lattice defects in bcc Fe [23,25,30–32]. These are: (i) the pairwise Johnson potential (henceforth referred to as '*J*') used already in a series of studies addressing the interaction of a ½⟨1 1 1⟩{1 1 0} edge dislocation, SIA clusters and vacancies with a carbon [23,31,32]. (ii) EAM-type potential developed by Becquart and Raulot (henceforth will be referred to as '*R*') [25], which is adjusted to a set of *ab initio* data on carbon–vacancy and carbon–carbon interaction.

Among the listed potentials, the *H* potential is the only one that was adjusted to describe a specific angular dependent carbon–carbon interaction in bulk Fe and correctly reproduces a strong repulsion of carbon in the vicinity of a ⟨1 1 0⟩ dumbbell. Yet, the *R* potential reasonably reproduces the C–C interaction in comparison with DFT data, as shown in [25]. Both *R* and *J* potentials predict a strong positive binding energy (C – ⟨1 1 0⟩) whereas a negative one is predicted according to the DFT calculations (see Table IV in Ref. [27]). All used potentials have the same Fe–Fe part from Ref. [33], which is known to be one of the best EAM-type potentials describing properties of iron and its lattice defects. All used potentials predict the octahedral site for carbon to be the most stable position and the relative difference with respect to the tetrahedral site is 0.85–0.9 eV. The corresponding carbon migration energy barrier is 0.86, 0.85 and the saddle point is the tetrahedral site for the *J* [31] and *R* [25] potentials. The actual migration path for the *H* potential has not been reported in the original work thus the migration energy, calculated as the energy difference between octa- and tetrahedral sites, is assumed to be 0.89 eV. We return to this point in Section 4. The carbon solvation energy in the Fe matrix (i.e. the difference in the crystal energy with and without carbon atom), is significantly underestimated by the *J* potential (1.23 eV) in comparison with the two other potentials, giving 10.05 (*R*) and 6.27 (*H*) eV. The potential by Hepburn, however, was fitted to reproduce the solvation energy as found in DFT calculations.

3.2. Molecular static simulations

Molecular static (MS) relaxation techniques were used to characterize the interaction of C with interstitial and vacancy defects in a bcc Fe matrix. A combination of conjugate gradient potential energy minimization and quasi-dynamic quenching was applied to relax the atomic configurations and to calculate the total potential energy of crystals (E_T) at zero temperature. The corresponding interaction energy (E_I) of two interacting entities (say A and B) making a complex AB was then derived according to the following definition:

$$E_I(A,B) = [E_T(AB) + E_T(\text{perfect})] - [E_T(A) + E_T(B)] \quad (1)$$

here E_T(A), E_T(B), E_T(AB) are the total energies of the relaxed crystal containing either defect A, B or the complex AB. E_T(perfect) is the total energy of a perfect crystal to respect the balance in terms of number of Fe atoms involved in the calculations of E_T(A), E_T(B), E_T(AB). According to this definition, a negative E_I implies attractive interaction between defects A and B. Then, the dissociation energy, E_D(A,B) for a defect A bound to B can be calculated as the difference of the migration energy, E_M(A), and interaction energy, E_I(A,B). If both defects A and B are mobile and have different migration energies, E_D(A,B) is not equal to E_D(B,A) and the effective dissociation energy is the lowest one. If a complex contains three or more elementary defects (e.g. v–C_2) different dissociation mechanisms are possible but the most probable one requires the lowest E_D.

It is convenient to use the concept of interaction energy when the considered defects exhibit both attractive and repulsive interaction, as in the case of Carbon and a dislocation. If only attraction is present (e.g. vacancy–Carbon), it is handy to measure the interaction strength in terms of binding energy (E_B), which is the negative of E_I. In the following, we shall use both terms depending on the type of interacting defects considered.

Calculations were performed in boxes containing up to 54 thousands atoms, depending on the size of the defect. The largest defect considered was a 61-SIA cluster with a hexagonal shape containing ⟨1 1 1⟩ crowdions and having its sides oriented along ⟨1 1 0⟩ directions. MS relaxations were performed at constant volume and 3D periodic boundary conditions were applied. The integration time step for quasi-dynamic quenching was varied from 0.1 up to 2 fs, depending on the potential applied. When the *H* potential was used, the time step was decreased down to 0.01 fs to achieve a proper relaxation. Small SIA and vacancy clusters were studied in a cubic box with principal axes oriented along the [1 0 0], [0 1 0] and [0 0 1] directions. Large ⟨1 1 1⟩ SIA clusters were considered using parallelepiped-like boxes with principal axes oriented along [1 1 1] [1 1 −2] and [1 −1 0] directions, with an elongation along the [1 1 1] direction to accommodate the strain.

3.3. MD simulations

To study the interaction of carbon and v–C complexes with a ½⟨1 1 1⟩ loop, the so-called 'loop-drag' model [28] was applied. In this model, an MD system contains a ½⟨1 1 1⟩{1 1 0} edge dislocation and a loop with the same Burgers vectors placed below the dislocation, as shown in Fig. 1. The principal axes of the box coincide with the [1 1 1], [1 1 −2] and [1 −1 0] directions. Periodic boundary conditions were imposed along *x* and *y* directions, whereas atoms in the upper and lower parts of the box were fixed with free surface boundary conditions [34]. Such a model considers a periodic array of edge dislocations and an infinite row of dislocation loops. The crystal used in the calculations has dimensions L_x = 12.5 nm, L_y = 15 nm and L_z = 16.5 nm, which corresponds to a dislocation density of 5×10^{15} m^{-2}. The chosen size of the crystal was checked to be sufficiently large to avoid any significant interaction between the dislocation and loop with their images.

The cluster is placed below the glide plane at a distance of about 5 nm. The position of a carbon atom or v–C complex was varied with respect to the glide prism of the loop. A defect is initially placed at a distance of about 10 nm away from the SIA cluster (along *x* axis). This system is first relaxed and then thermalized using quench and velocity rescaling algorithms, respectively. Then an external load is applied by shearing the upper block of the crystal containing immobile atoms, as it is done in the original model for the edge dislocation described in [34]. Under shear strain applied with a constant rate, the dislocation moves and drags the SIA cluster allowing the study of carbon–cluster interaction in dynamics. The interaction is expressed in the change on the flow stress for the unpinning of the loop from a given defect

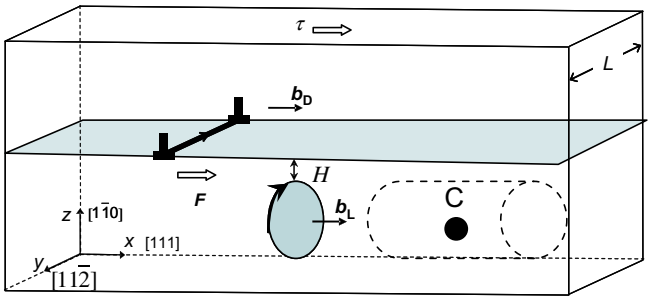

Fig. 1. Schematic picture of a ½⟨1 1 1⟩{1 1 0} edge dislocation–dislocation loop MD setup used to study the interaction of a ½⟨1 1 1⟩ loop with carbon, v–C and C–C complexes. The dislocation and loop have the same Burgers vectors $\boldsymbol{b}_D = \boldsymbol{b}_L = ½[1\,1\,1]$. Line sense for the dislocation and dislocation loop is shown by an arrow on the figure.

simultaneously calculated during the simulation, which can be a measure of the interaction energy. Important to note is that the dislocation is placed far enough to not exhibit any significant interaction with a carbon or v–C complex, as was checked by a separate set of calculations excluding the loop.

Simulations were performed in the temperature range 50–800 K and the lattice parameter was adjusted to maintain zero pressure in the system at each temperature. MD simulations were performed in the NVE ensemble without additional temperature control. The MD time step was varied from 1 up to 4 fs depending on temperature. The increase of the temperature, due to the dissipation of the energy of the moving dislocation, was insignificant, i.e. a few Kelvin for the longest run.

4. Results

The results are presented in two sections, containing data obtained from MS and MD simulations, respectively. Static calculations were performed to characterize the interaction of a carbon atom in octahedral interstitial position with vacancy clusters of sizes from 2 to 6, small parallel and non-parallel SIA clusters made of ⟨1 1 0⟩ dumbbells of sizes from 2 to 5 and larger SIA clusters of hexagonal shape, made of ⟨1 1 1⟩ crowdions containing 7, 19 and 61 SIAs. MD simulations were used to consider the mechanism of interaction of an isolated carbon atom, carbon–vacancy (v–C) and carbon–carbon (C–C) complexes with a ½⟨1 1 1⟩ dislocation loop, moving under stress acting from the edge dislocation in a loaded crystal.

However, prior to present the main results we calculate the migration energy of C using the *H* potential. The migration path calculations were performed at fixed volume using a plane-constrained relaxation within the standard drag method (see e.g. [35]). The results for the *H* and *R* potentials are presented in Fig. 2a (note that the profile for *J* is almost identical to *R*). While the profile for the *R* potential agrees well with the one published in [25], we see clearly that the saddle point configuration, according to the *H* potential, is not a tetrahedral position. The actual energy barrier is 1.3 eV and not 0.89 eV. In addition, there is a metastable state, which a Carbon atom occupies while moving towards a tetrahedral position.

Furthermore, we have applied MD to study thermally activated motion of an interstitial C atom. Simulations were performed in an MD box containing 2000 bcc lattice sites with constant volume and periodic boundary conditions at $T = 1000$, 1200 and 1500 K. The diffusion coefficient was estimated over the simulation time of 10 ns and the corresponding Arrhenius plot is drawn in Fig. 2b. The corresponding migration energy and prefactor of the diffusion coefficient were calculated to be 1.0 ± 0.07 eV and 4.04×10^{-6} m^2/s for the *H* potential and 0.65 ± 0.25 eV and 1.95×10^{-7} m^2/s for the RAU potential. The estimated migration energy is lower than the static value, which is consistent with the results obtained using the *J* potential [36]. The calculated prefactor also reasonably agrees with the value 1.89×10^{-7} m^2/s given in [36]. Thus, according to the *H* potential, the actual migration energy of Carbon is higher than the energy difference between octa- and tetrahedral configurations. This is clearly an essential drawback, which was not mentioned in the original work and for which we shall discuss the possible impact later in Section 5. In the following, for the *H* potential we shall consider the migration energy of C to be 1.3 eV as obtained from the static simulations.

4.1. Static simulations

As mentioned in Section 3.1, only the *H* potential correctly reproduces the C – ⟨1 1 0⟩ dumbbell interaction, thus we only use this potential to consider the interaction of a carbon atom with

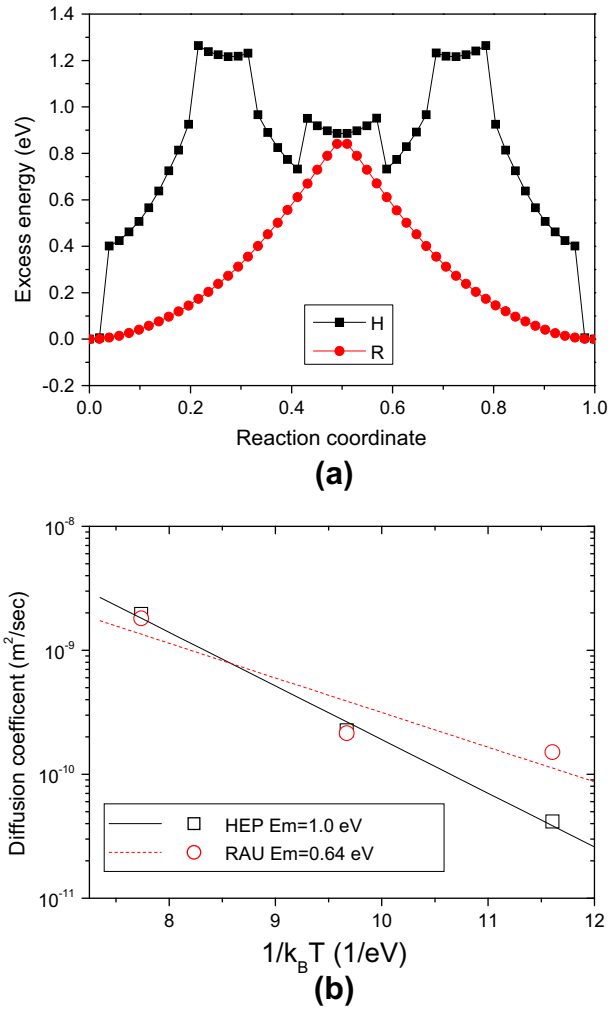

Fig. 2. (a) Minimum energy path for the migration of a Carbon atom between two octahedral sites passing through a tetrahedral site calculated using the *H* and *R* potentials. (b) Temperature dependence of the C atom diffusion coefficient.

⟨1 1 0⟩ SIA clusters and non-parallel clusters containing less than 6 SIAs.

All possible octahedral positions near an SIA cluster of a given size were scanned within a distance of the 3rd nearest neighbour shell from each dumbbell forming a cluster. MS simulations performed using the *H* potential have shown that a carbon atom does not have a positive binding energy with ⟨1 1 0⟩ SIA clusters with size up to five defects. The configurations of the studied SIA clusters were taken from Ref. [6], where the lowest energy structures were determined. No positive binding energy was found between a carbon and non-parallel clusters, whose structures are reported in Ref. [29]. In all cases a negative binding energy varying from 0.1 up to 0.3 eV was obtained for a carbon placed within the 1st nearest neighbour distance from any SIA forming the cluster. A weak positive binding energy (i.e. attractive interaction) of about 0.02–0.05 eV (depending on the cluster size and configuration) was found for a carbon atom placed at a distance corresponding to the 3rd nearest neighbour shell. We conclude that carbon atoms do not act as traps for small ⟨1 1 0⟩ or non-parallel SIA clusters, and do not stabilize them.

4.1.1. Interaction of carbon with ½⟨1 1 1⟩ SIA clusters

The interaction energy between a carbon and the 7-SIA cluster made of ⟨1 1 1⟩ crowdions was calculated for every octahedral

position in the habit plane of the cluster. The energy maps were constructed for each potential and are shown in Fig. 3. The figure shows all octahedral positions in the (1 1 1) plane and the 7-SIA cluster is placed in the middle. The results show that C has the lowest interaction energy with the cluster when placed just outside of the cluster's edge. All maps in Fig. 3 show the same qualitative but different quantitative information. The lowest interaction energy (i.e. the strongest attraction) −0.47 eV is found with the *H* potential, being −0.39 eV and −0.43 eV, for *R* and *J* potentials, respectively. Additional calculations were done for a carbon placed at different distances away from the habit plane to estimate the interaction range. The distance at which the attractive interaction vanishes was found to be ~10***b*** (here ***b*** is $\sqrt{3}/2a_0$).

Considering the interaction of a carbon with larger ⟨1 1 1⟩ clusters, which can be described as ½⟨1 1 1⟩ dislocation loops, we also found that the strongest attractive interaction occurs for C placed at the periphery of the cluster, but not necessarily outside the cluster's glide prism. The sign of the interaction was found to depend on the interatomic potential and specific position of carbon with respect to the tetragonal distortion axis (TDA). In addition, the strength of the interaction depends on the specific position of the carbon atom with respect to the corner of the cluster. For a given lattice site there are two non-equivalent octahedral positions defining a specific tetragonal distortion axis. One position coincides with the trace of a {1 1 0} atomic plane (henceforth called TDA[0 0 1]) and another one lays between two non-equivalent {1 1 0} atomic planes (henceforth called TDA[1 0 0]/[0 1 0]). The results obtained with the *J* and *R* potentials were found to be qualitatively and quantitatively the same. Therefore, in the following we report only data obtained using the *R* and *H* potentials, where significant differences were observed.

According to the *J* and *R* potentials, a repulsive interaction occurs within the cluster's glide prism, which changes to an attractive interaction outside the glide prism, in the tensile region of the cluster. A somewhat unexpected result was found with the *H* potential, according to which an attractive interaction also exits in the compressed region. Profiles of the interaction energy between an octahedral C and ⟨1 1 1⟩ 61-SIA cluster calculated with the *H* and *R* potentials are presented in Fig. 4a, for the TDA[0 0 1] position. E_I is plotted as a function of the position of C on a line perpendicular to the cluster's habit plane. The line intersects the cluster at the middle of the side and passes outside the glide prism. The *H* potential predicts an attractive interaction with binding energy 0.5 eV and 0.6 eV in the tensile and compressed regions, respectively. In turn, the *R* potential suggests the attraction only in the tensile region with a maximum binding energy of 0.4 eV. Both potentials predict approximately the same interaction range along the Burgers vector direction, which is about 10***b***. Note that at a distance larger than 4***b*** there is a weak repulsive interaction (0.15 eV). Changing the orientation of the TDA does not affect the maximum attraction energy but results in an increase of the maximum repulsion energy up to 0.4 eV according to both potentials. The same calculations performed with the *H* potential, placing C near a corner of the 61-SIA loop, as schematically shown in the inset of Fig. 4b, have shown that the maximum attractive energy can reach 0.65 eV (see Fig. 4b). A detailed map for the interaction energy in the habit plane of the 61-SIA cluster is presented in Fig. 5 for the so-called 'upper' and 'lower' regions of the loop. The need to characterize both sides of the loop appears because the loop habit plane is slightly tilted towards a {1 1 0} plane. Because of this, the determination of the most energetically favourable position for Carbon near the loop requires considering few {1 1 1} planes.

Given the significant difference between the results for the interaction of Carbon with the loop segment obtained for the compressed region using the *R* and *H* potentials, we have considered the interaction of Carbon with a straight ½⟨1 1 1⟩{1 1 0} edge dislocation. The interaction energy versus distance between C and the edge dislocation is presented in Fig. 6 for the two non-equivalent TDA positions. The position of Carbon with respect to {1 1 0} atomic planes is schematically shown in the figure too. We see that the maximum binding energy (*H* = 0.68 eV and *R* = 0.64 eV) occurs when Carbon is placed in the tensile region in the TDA[0 1 0] position. At the compressed region, it is only the *H* potential which predicts attraction of 0.46 eV (also for the TDA[0 1 0] position). When applying the *R* and *J* potentials and placing C in the compressed region near the dislocation core, the dislocation was seen to be unstable in its initial position and glided away (overcoming a couple of Peierls valleys) from C during the relaxation. The resulting interaction energy was estimated to be 0.05 eV (i.e. repulsive interaction) for both potentials.

Thus, the *H* potential predicts a qualitatively different result in the cases of large SIA clusters and the edge dislocation as compared to the data obtained with the *R* and *J* potentials, which do not show any attractive interaction for C placed in the compressed region of the edge dislocation or dislocation loop.

4.1.2. Interaction of carbon with vacancy defects

In the following we present the results of MS calculations concerning the interaction of a carbon atom with small (mobile) vacancy clusters containing up to six vacancies. Vacancies in the cluster were arranged in the configurations corresponding to the lowest energy state. As in the case of the calculations involving SIA clusters we have scanned all possible octahedral positions near a vacancy cluster of a given size. The most energetically favourable

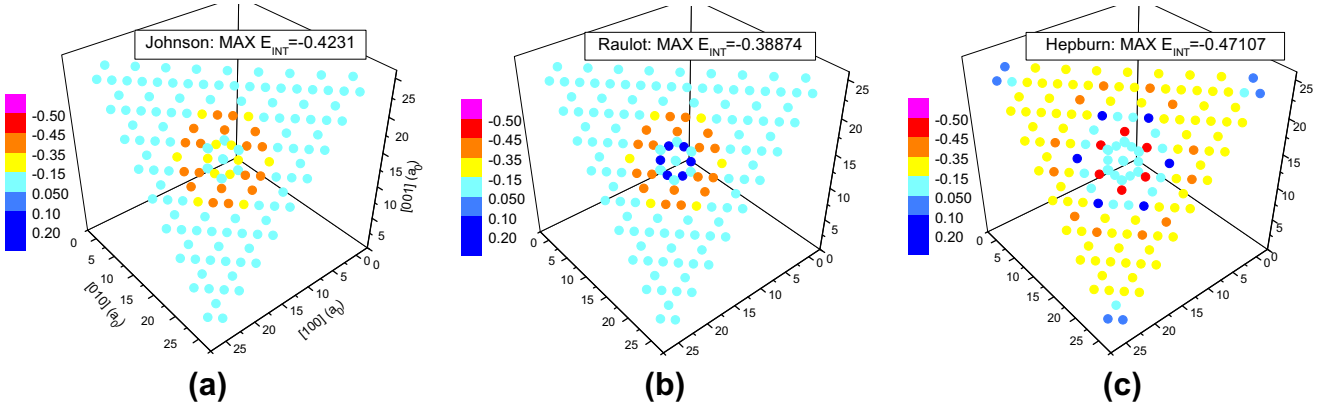

Fig. 3. Interaction energy maps for a C–7 SIA cluster complex drawn in the cluster's habit plane, calculated using (a) Johnson, (b) Raulot and (c) Hepburn Fe–C potentials.

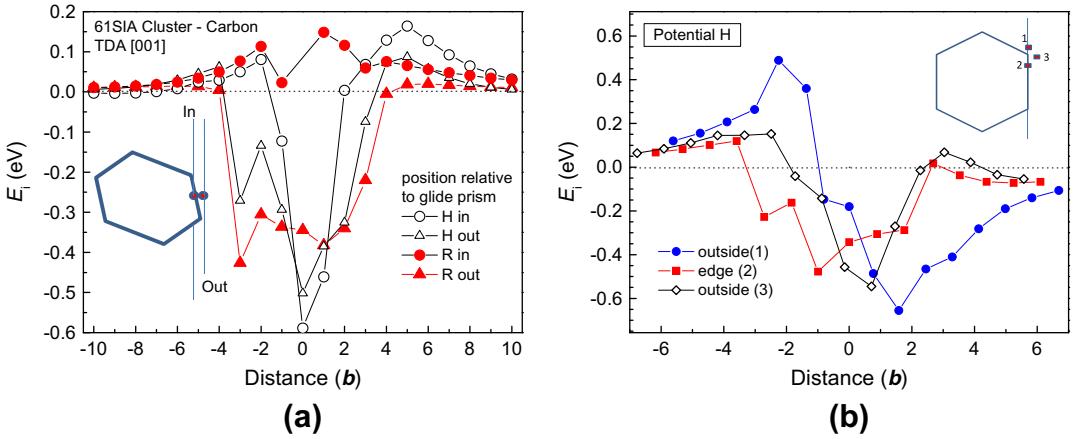

Fig. 4. Interaction energy between a carbon atom and 61-SIA cluster versus distance to the cluster habit plane. A carbon atom was placed in different positions along the [1 1 1] axis crossing the cluster: (a) in the middle of its side. 'In' = inside the glide prism; 'out' = outside the glide prism; (b) at its corner, as shown on the inset drawings. Data shown in (a) are obtained using the *R* and *H* potential, while data shown in (b) are obtained using the *H* potential only.

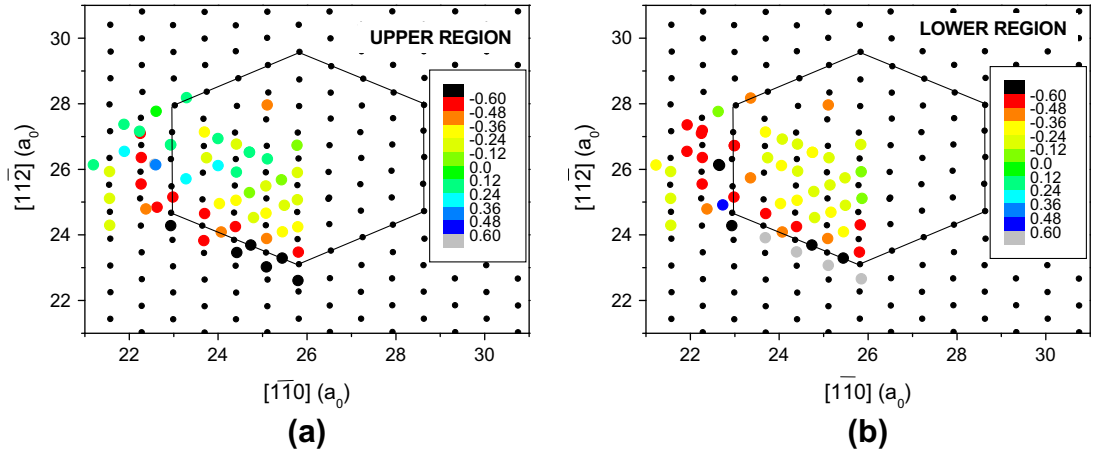

Fig. 5. Interaction energy maps calculated for a 61-SIA cluster using the *H* potential. The maps are calculated for (a) the 'upper' and (b) 'lower' parts of the cluster (see explanations in the text).

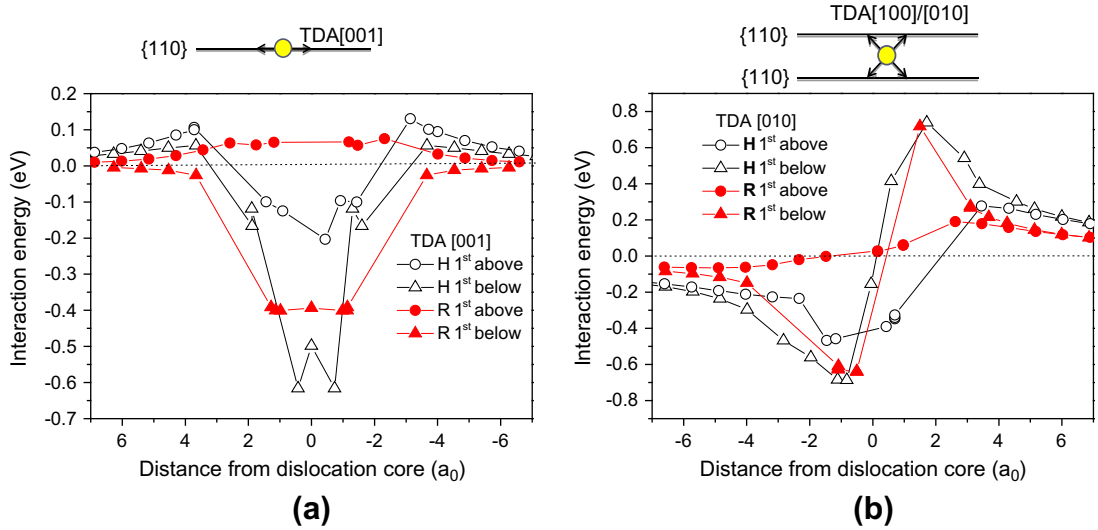

Fig. 6. Interaction energy versus distance between carbon and the core of a ½⟨1 1 1⟩{1 1 0} edge dislocation. The data are obtained using the *R* and *H* potentials for the two different TDA positions of carbon, namely: (a) [0 0 1] and (b) [0 1 0] (see explanation in the text for the difference).

v_N–C configurations, obtained with the three potentials, are displayed in Fig. 7. All potentials predict that the optimal C–vacancy arrangement is achieved when C is located at the first nearest octahedral site relative to a vacancy (see Fig. 7a). According to the *H* potential, a carbon atom prefers to reside next to di- and tri-vacancy clusters (see Fig. 7b and c). In the case of the four-vacancy cluster a weak attractive interaction is found only if C is placed at a considerable distance away from the cluster (see Fig. 7d). For the larger clusters the lowest energy of the system was obtained when a carbon atom was placed away from the cluster. On the contrary, a carbon atom is attracted to a vacancy cluster irrespective of its size, according to the *J* and *R* potentials (see Fig. 7d–f). Interesting to note, none of the potentials predict the presence of a carbon inside the vacancy clusters to be energetically favourable.

Quantitative assessment of the interaction between carbon and vacancy clusters is presented in Fig. 8 in terms of E_B and E_D, calculated separately for a carbon atom (Fig. 8a and c), vacancy (Fig. 8b and d) and vacancy cluster (Fig. 8f). The migration energy for a single vacancy, carbon atom and vacancy cluster containing up to six vacancies, used to calculate the dissociation energies, are displayed in Fig. 8e. The data for vacancy clusters was taken from Ref. [37]. The *J* and *R* potentials predict similar trends for both interaction and dissociation energies, so that E_D for a vacancy grows monotonically with the cluster size, whereas E_D for C does not essentially depend on the cluster size. The absolute values of E_D for the dissociation of a vacancy are almost identical with the two potentials (see Fig. 8d), whereas E_D for a carbon atom is systematically higher by ~0.25 eV with the *R* potential (see Fig. 8c). The *H* potential predicts E_D for a carbon atom to be in between the data obtained with the other two potentials. The dissociation energy of a vacancy from a v_N–C, calculated with the *H* potential, is in qualitative but not quantitative agreement with other potentials, see Fig. 8f.

The most probable dissociation reactions and corresponding energies, calculated based on the results presented in Fig. 8, are summarized in Table 1. The breakup of a v–C pair requires 1.48 eV according to the *R* potential, which is higher by ~0.3 eV as compared to E_D(v–C) obtained with the other two potentials. Concerning v_N–C complexes, all potentials suggest that the dissociation energy increases with the cluster size. It is only the *R* potential that predicts the dissociation of v_N–C complexes to occur via emission of a single vacancy. According to the *H* and *J* potentials, the breakup of v_3–C, v_4–C and v_6–C should occur via detaching of a vacancy cluster from a carbon, which is not surprising given that the migration energy of small vacancy clusters is even lower than that of a single vacancy.

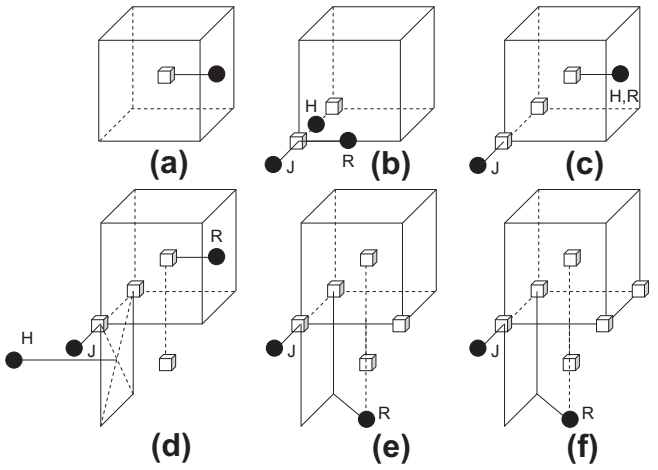

Fig. 7. The energetically most favourable C–v_N configurations calculated for the three potentials. The position of a carbon atom in each cluster, corresponding to its lowest energy configuration, is marked by the first letter of the corresponding potential.

Finally, we present quantitative characterization of the di-carbon–vacancy (v–C_2) complexes which are believed to be stable up to relatively high temperature and therefore can contribute to the retardation of the motion of 1D mobile SIA clusters. The interaction and dissociation energy for a vacancy and carbon atom entering two complexes named 'linear' and 'adjacent' are presented in Fig. 9. The arrangement of carbon atoms in these complexes is shown on the inset figures. We present the results obtained with the three potentials, even though the *J* potential does not consider C–C interaction. Yet, we note that the *J* and *H* potentials predict similar results, although the former overestimates E_I(C + v–C) and hence overestimates the dissociation energy for a carbon atom leaving v–C_2. The *H* potential incorrectly predicts the migration energy for C (see Fig. 2) and therefore also overestimates E_D for a carbon atom (for both linear and adjacent configurations). The *R* potential does not predict attractive interaction between C and v–C complex for the adjacent configuration, contrary to the other potentials. The binding energy of a vacancy with di-carbon complex is predicted to be higher for the linear configuration, according to all potentials. Based on the obtained results we conclude that the most probable reaction for the dissociation of a v–C_2 complex, no matter linear or adjacent configuration, is the emission of a carbon atom. The only exception is the adjacent configuration treated with the *H* potential, according to which the emission of a vacancy should cost a smaller amount of energy. The corresponding dissociation energies are reported in Table 1. Note that the rather small dissociation energy for the adjacent configuration obtained with the *R* potential stems from the fact that C is not attracted to the v–C complex to form the adjacent configuration, which is due to the strong C–C repulsion at distances smaller than a_0. This repulsion is much weaker with the *H* potential and does not exist at all in the *J* model, because of the absence of C–C interaction.

4.2. Dynamic simulations

The results of static simulations presented in Section 4.1.1 have shown that depending on the position of a carbon atom with respect to the glide prism of a ½⟨1 1 1⟩ loop, C may act either as a trap or repulsive center. In both cases, the presence of C on the way of a gliding ½⟨1 1 1⟩ loop should retard its movement. In the two following sections we describe results obtained from MD simulations where the interaction of a carbon and carbon–vacancy complexes with a ½⟨1 1 1⟩ 61-SIA loop was considered. The loop was dragged by a ½⟨1 1 1⟩{1 1 0} edge dislocation (located above the loop, as shown in Fig. 1), whose movement was induced by applied shear strain at constant rate. MD simulations have been performed only with the *H* potential presuming that it is the most reliable among the others with respect to the interaction with over-coordinated defects.

Two types of MD simulations were performed. Simulations addressing the problem of carbon-loop drag were performed at $T = 600$ and 800 K, applying a low strain rate of 10^6 s^{-1} (i.e. low for MD time/space scale), so that the dislocation velocity, v_D, was 0.8 m/s. The interaction of the loop with v–C and C–C complexes was studied at low temperature ($T = 50$ and 100 K) and relatively high strain rate 5×10^7 s^{-1} ($v_D = 40$ m/s), to reveal the impact of a given complex on the critical stress at which the loop is released from. An increase in the shear stress applied to the dislocation for the release of the loop gives a measure of the defect–loop interaction. The position of the complex was varied with respect to the loop's glide prism. In the absence of a defect, the loop was seen to be dragged by the dislocation at a stress not exceeding

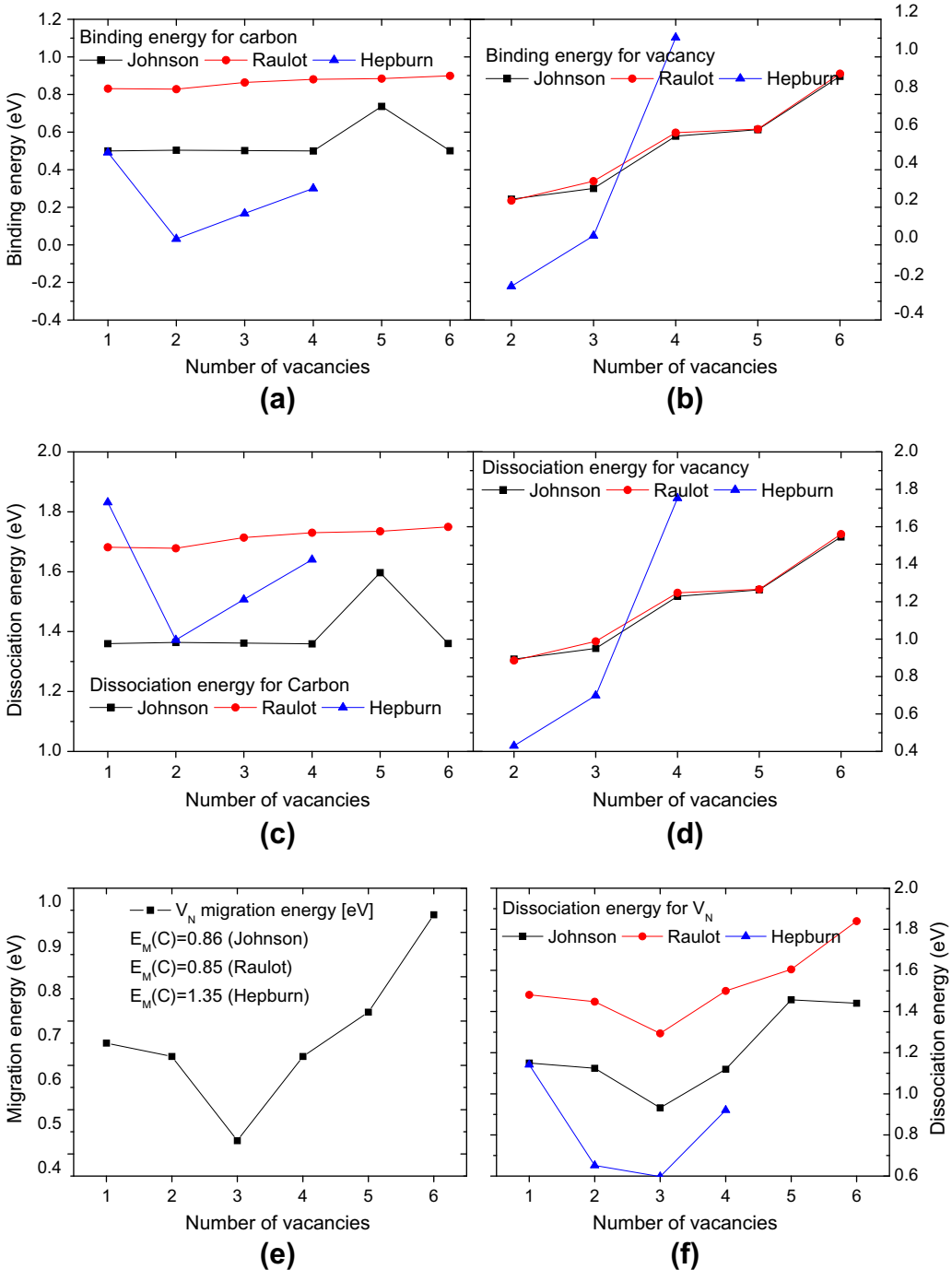

Fig. 8. The interaction energy and dissociation energy for C (a,c) and V (d,e) in v_N–C complexes containing different number of vacancies as a function of *N*. (e) The migration energy for a v_N cluster and (f) dissociation energy for a v_N cluster from a v_N–C complex as a function of *N*.

~5 MPa at the lowest temperature and highest strain rate considered here.

4.2.1. Interaction of a carbon atom and C–C pair with a ½⟨1 1 1⟩ dislocation loop

Four different interaction geometries were considered as shown in Fig. 10a and named as 'corner', 'center', 'side' and 'outside'. We recall that static simulations revealed only a weak repulsive interaction between a carbon and the 61-SIA loop in 'center', while a strong attractive interaction occurs in the positions called 'corner' and 'outside'. The strongest attraction is found for the position called 'outside' with $E_I = 0.6$ eV (see Fig. 4).

Let us first describe the results obtained at high temperature and low strain rate. In none of these simulations carbon-loop drag was seen. The interaction time (i.e. time before the loop was released from a carbon) and critical stress are summarized in Table 2. The interaction mechanism and ability of a carbon to move during the reaction was found to depend on its position relative to the loop's glide prism. At 600 K, the movement of carbon was only registered in the reaction when C was initially placed at the corner. Then, it jumped inside the glide prism before unpinning. At 800 K, movement of a carbon atom along the side of the loop was registered if it was placed in the position called 'side'. Displacement of a carbon atom from 'outside' and 'corner'

Table 1
Dissociation reaction and corresponding binding and dissociation energy for v_N–C and v–C_2 complexes calculated with different potentials. (*) Shows the energetically most favourable v–C_2 configuration.

v_N–C complex	Dissociation reaction	Binding energy (eV)	Dissociation energy (eV), the migrating object is specified in the brackets
J potential			
v–C	v + C	0.5	1.15
v_2–C	v + v–C	0.24	0.89
v_3–C	v_3+C	0.50	0.93 (v_3)/0.95 (v)/1.36 (C)
v_4–C	v_4+C	0.5	1.12 (v_4)/1.22 (v)/1.36 (C)
v_5–C	v + v_4–C	0.61	1.26
v_6–C	v_6 + C	0.50	1.44 (V_6)/1.54 (v)/1.36 (C)
v–C_2 (linear)	C + v–C	0.50	1.36
v–C_2 (adjacent)*	C + v–C	0.50	1.36
R potential			
v–C	v + C	0.83	1.48
v_2–C	v + v–C	0.24	0.88
v_3–C	v + v_2–C	0.34	0.99
v_4–C	v + v_3–C	0.60	1.25
v_5–C	v + v_4–C	0.62	1.27
v_6–C	v + v_5–C	0.91	1.56
v–C_2 (linear)*	C + v–C	0.29	1.14
v–C_2 (adjacent)	C + v–C	−0.32	0.53
H potential			
v–C	v + C	0.49	1.14
v_2–C	v + v–C	−0.22	0.43
v_3–C	v_3 + C	0.17	0.6 (v_3)/0.69 (v)/1.5 (C)
v_4–C	v_4+C	0.30	0.92 (v_4)/1.75 (v)/1.65 (C)
v–C_2 (linear)*	C + v–C	0.17	1.51
v–C_2 (adjacent)	C–C + v	0.12	1.23

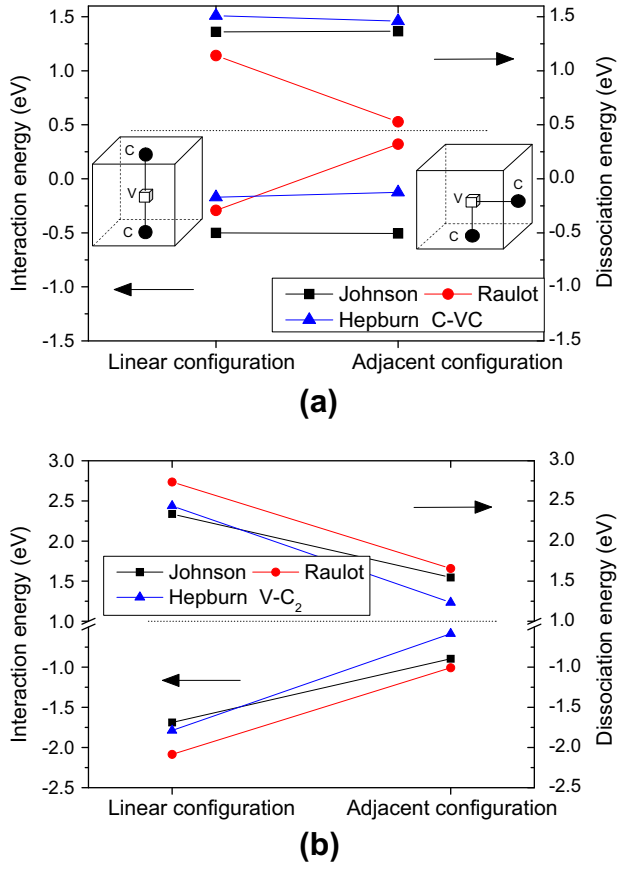

Fig. 9. The interaction and dissociation energies for a carbon (a) and vacancy (b) in a v–C_2 complex arranged in the linear and adjacent configurations.

positions during the interaction at 800 K was also observed. In these reactions C moved to occupy an octahedral position on the edge of the loop inside the glide prism. Although movement of C along the loop side was registered at T = 800 K, no continuous displacement of a carbon-loop complex was observed. A few jumps of carbon along the loop side were registered during a simulation time of ~10 ns, which suggests that the mobility of a carbon atom near the edge of the loop can indeed be enhanced.

Interaction time, critical resolved shear stress at the moment of release and a brief description of the interaction mechanism are presented in Table 2. We see that the critical stress for the release is not high and thus an isolated carbon cannot be considered as a strong obstacle for the propagation of a ½⟨1 1 1⟩ 61-SIA loop. Few jumps of Carbon along the side of the loop were registered in several simulation runs (see Table 2). The interaction of a C–C pair located either in the 'corner' or in the 'side' positions, as schematically shown in Fig. 10b and c, was also modeled at 600 K to see whether the interaction is additive or not. The critical stress almost did not change. Detailed analysis of the reaction revealed that the two opposite sides/corners of the loop released from the carbon atoms independently (i.e. not simultaneously). By increasing temperature from 600 to 800 K, we also observed a slight change of the unpinning stress. The change of the unpinning stress is, however, within the 'noise' arising from thermal fluctuations.

The effect of a strong interaction on the unpinning stress is well seen in low temperature simulations, where a carbon atom was not observed to move during the reaction. Fig. 11a presents stress–strain curves obtained in simulations done at 50 K for C placed in the positions 'center' and 'corner'. The attractive interaction between C and the loop ($E_I \sim 0.6$ eV) requires an application of 126 MPa for the loop to pass the obstacle. A release of the loop from C located in the 'center' position ($E_I \sim 0.15$ eV) occurs at stress of about 25 MPa. We thus see that there is a correspondence between the interaction energy and unpinning stress in the low temperature simulations. Simulations repeated in the same conditions with two carbon atoms placed in the 'corner' positions have shown that the critical stress increases approximately as twice.

4.2.2. Interaction of {v–C_m} complexes with a ½⟨1 1 1⟩ dislocation loop

The studied {v–C_m} complexes (m = 1, 2), their orientation and location relative to the loop's glide prism are shown in Fig. 10d–f. Only low temperature MD simulations (50 and 100 K) were

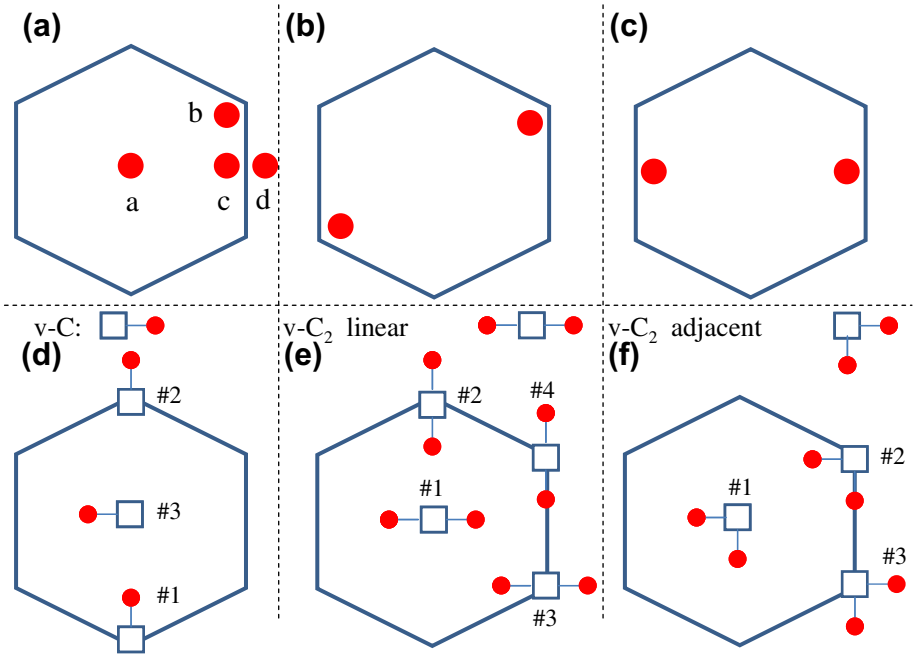

Fig. 10. Interaction geometry for the reactions between a ½⟨1 1 1⟩ 61-SIA loop and an isolated carbon atom (a), a pair of carbon atoms (b,c), v–C (d) and v–C_2 (e,f) complexes, studied using low temperature MD simulations. The configurations for v–C_2 called 'linear' and 'adjacent', schematically drawn in (e) and (f), are shown in detail as insets in Fig. 9a.

Table 2
Interaction time, critical resolved shear stress at the moment of release and brief description of the interaction mechanism.

	Time (ns)	Details of interaction/carbon movement	$\int_{max}$ (MPa)
1C corner T = 600 K	9.8	Carbon jumped away from the corner inside the glide prism towards the center of the loop	28
1C corner T = 800 K	3	Carbon jumped away from the corner towards the middle of the side	25
1C side T = 600 K	11.5	No movement of carbon was seen	22
1C side T = 800 K	3	Carbon jumped outside of the glide prism	17
1C outside T = 600 K	16.1	Carbon was seen to jump along the loop side	32
1C outside T = 800 K	6.4	Carbon was seen to jump along the loop side	36
2C corner T = 600 K	16.1	One carbon atom was seen to migrate towards the middle of the loop side	25
2C side T = 600 K	13.5	One carbon atom jumped in the [1 1 1] direction, coinciding with the direction of the dislocation motion. Another Carbon was also seen to jump in the [1 1 1] direction and migrate to the corner of the loop	18
1C side T = 50 K		No movement of carbon was seen	23
1C outside T = 50 K		No movement of carbon was seen	126

performed. The resulting interaction mechanism and unpinning stress for the reactions done at 50 K are summarized in Table 3. Stress–strain curves for some of the reactions considered are shown in Fig. 11b.

When the complexes were placed in the center of the glide prism, the critical stress was only slightly higher than the one measured in the reaction with an isolated carbon. In all of these cases the loop passed through the complex without modifying its structure. If the {v–C_m} complex intersects with a side or corner of the loop, the interaction is much stronger. Over all studied configurations, the minimum unpinning stress is 100 MPa and the maximum is about 210 MPa. In these cases, a vacancy entering the {v–C_m} complex was absorbed during the interaction time. In the reaction with the linear configuration of the v–C_2 in the position #4 (see Fig. 8e), the loop was detached from the dislocation i.e. left behind the moving dislocation (this was also observed in simulations at 100 K). The moment at which the dislocation was unpinned from the loop is clearly seen in Fig. 11b because the stress becomes negative, due to the bending out of the released dislocation. Thus, the measured critical stress corresponds to the detachment of the dislocation from the loop, therefore the stress needed for the loop to overcome the v–C_2 cluster is even higher.

We did not perform dedicated MS simulations to characterize the interaction energy map for the studied {v–C_m} complexes as the number of possible configurations is huge. Regarding the obtained unpinning stresses one can roughly estimate the interaction energy for the reactions with the linear configuration of v–C_2 in positions #2 and #4 to be about two times higher than E_l for an isolated carbon in the position 'corner'. It means that its absolute value would be of the order of 0.9–1 eV. Another important aspect of the interaction of v–C_2 complexes with ½⟨1 1 1⟩ dislocation loops is that prior to the contact there is a relatively long-range attractive interaction between them because of the presence of a vacancy in the complex. One can therefore expect that the loop would be attracted to such complexes.

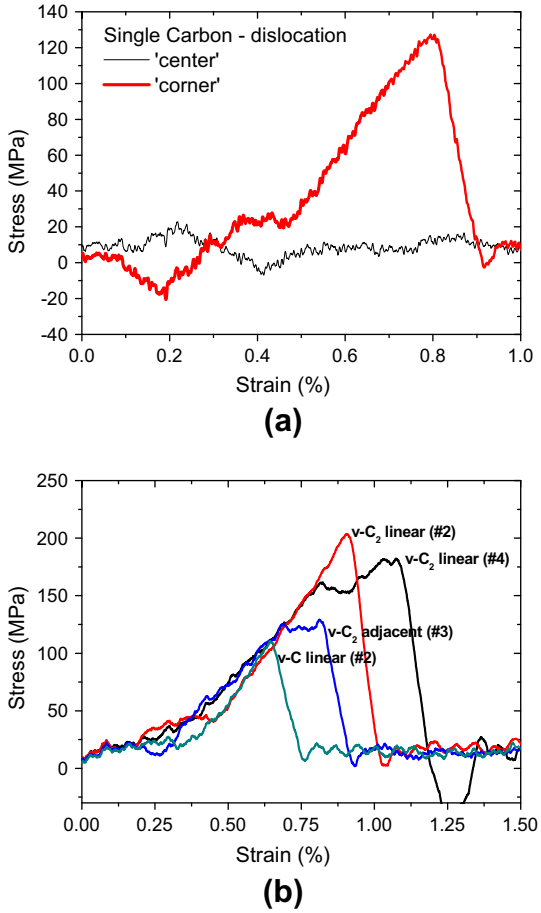

Fig. 11. Stress–strain curves corresponding to the interaction of a ½⟨1 1 1⟩ 61-SIA loop with (a) an isolated carbon atom located in the positions 'center' and 'corner' and (b) with v–C and v–C_2 complexes. Positions of the v–C complexes relative to the glide prism can be found in Fig. 10.

Table 3
Interaction mechanism and unpinning stress (τ_U) in the reaction between a ½⟨1 1 1⟩ 61-SIA loop and C–v complexes.

Configuration	Description of reaction	τ_U at $T = 50$ K (MPa)
2CV_adj_C1 (fig. f #1)	Complex remained unchanged	42
2CV_adj_C2 (fig. f #2)	Vacancy was absorbed, Carbon atoms occupy 3rd nn octahedral sites ($R = a_0$)	120
2CV_adj_C3 (fig. f #3)	Vacancy was absorbed, Carbon atoms occupy the same positions as before reaction	132
2CV_C1 (fig. e #1)	Complex remained unchanged	34
2CV_C2 (fig. e #2)	Vacancy was absorbed, Carbon atoms occupy the same positions as before reaction	210
2CV_C3 (fig. e #3)	Vacancy was absorbed, Carbon atoms occupy the same positions as before reaction	104
2CV_C4 (fig. e #4)	The loop did not unpin	184
CV_C1 (fig. d #1)	Vacancy was absorbed	97
CV_C2 (fig. d #2)	Vacancy was absorbed	114
CV_C3 (fig. d #3)	Vacancy was not absorbed	33

5. Discussion

5.1. Interaction of C with vacancy clusters

The interaction of C and C–C pair with a single vacancy has already been studied using the three potentials considered in the works [23,25,27]. For the *R* potential, it was found that the configurations involving one vacancy and one or two carbon atoms are generally in line with the DFT data, but the accuracy to reproduce specific binding energies is not always good. For instance, the *R* potential (i) overestimates by about ~0.4 eV the binding energy for a v–C pair in its lowest energy state; and (ii) underestimates significantly (by 1 eV) the total (i.e. for all entities) binding energy for the adjacent configuration of the v–C_2 cluster, as compared to DFT results [27]. The *H* potential, being derived to solve the problem of covalent bonding interaction, correctly predicts the total binding energy for the adjacent configuration (see right-hand inset on Fig. 9), but on the other hand, underestimates the total binding energy for the linear configuration (see left-hand inset on Fig. 9) by 0.5 eV. More importantly, the migration energy for an interstitial carbon atom is strongly overestimated (by ~50%, see Fig. 2) by the *H* potential. These discrepancies are important and will be recalled later on.

Another remarkable difference between the *H* potential and the two others consists in the arrangement of a carbon near vacancy clusters corresponding to their lowest energy states (see Fig. 7). No attractive interaction of C in the immediate vicinity of vacancy clusters containing 4, 5 and 6 vacancies was found with the *H* potential. Whereas both *J* and *R* potentials predict that C prefers to reside next to one vacancy forming a cluster. Here we have to mention that the most favourable v_N–C arrangement was searched by adding a C to the vacancy cluster configuration established to be the lowest energy state in pure Fe. We did not investigate whether the presence of a carbon atom could change the vacancy cluster structure, thus considering the situation where carbon atoms would reside on already formed vacancy clusters.

Regarding the binding and dissociation energies obtained using the three potentials for v_N–C clusters we can see that the *R* potential is the only one that predicts the dissociation to occur via the emission of single vacancies for all studied clusters. The corresponding dissociation energy increases from 0.88 up to 1.56 eV with cluster size. However, the *R* potential overestimates v–C binding energy by 0.4 eV, which affects the binding energy with vacancy clusters as well. With the *J* potential, the dissociation energy also increases with cluster size from 0.89 up to 1.36 eV. But both *H* and *J* potential suggest that the dissociation of V_3, V_4 and V_6 occurs via detachment of the cluster and carbon atom, contrarily to the *R* potential. The evaluation of the dissociation energy in this case is not unambiguous because it is known that the small vacancy clusters are mobile and their migration energies are lower than E_m(C) (see Fig. 8e). Hence, calculating the dissociation energy for a v_N–C cluster as a sum of the migration and binding energies, one can consider v_N cluster as the migrating object. Whether this mechanism can physically occur we do not know. The expression for the prefactor of the jump frequency to be used for such process is unclear as well. If we disregard the possibility for a vacancy cluster to leave a carbon atom and consider emission of C from a cluster, then in some cases the lowest dissociation energy would correspond to the evaporation of a vacancy and not a carbon atom. For convenience, we have reported the dissociation energy for all possible processes in Table 1.

We now can discuss the obtained results in the light of existing experiments dedicated to the study of vacancy–carbon interaction. As established from the DFT calculations, a vacancy–carbon pair has the dissociation energy of 1.12 eV, which is close to the vacancy migration energy, 1.28 eV, estimated in Fe containing limited concentration of carbon from high temperature measurements [38]. The results obtained with the *J* and *H* potentials are consistent with both DFT and experimental suggestions. In the annealing experiments combined with positron annihilation spectroscopy (PAS) measurements performed by Vehanen et al. [39] in Fe-doped specimens, evidence for the decoration of v–C pairs by additional carbon atoms was found. The dissociation of v–C_N

complexes (N could not be experimentally determined, but cannot be large because otherwise such complexes could not be identified by the PAS techniques) was registered at 490 K and the activation energy of 1.4 eV was assigned to this process. Above 500 K, only vacancy clusters remain and they anneal at 700 K. Resistivity recovery (RR) measurements followed by annealing done by Takaki et al. [19] suggested that in Fe–C doped specimens (i) vacancies (so called stage III defects) are trapped and immobilized by carbon atoms; (ii) v–C pairs act as saturable sinks for freely migrating carbon (presumably forming v–C_N complexes with N = 4–10); (iii) the dissociation of v–C_N complexes occurs at 580 K, with the activation energy of 1.55 eV. The latter is deduced by taking into account the heating rate and position of the stage following the expression suggested in [40].

We see that the results and their interpretations are consistent in the two above mentioned independent experimental works. The dissociation energies for v–C_2 complexes obtained here fall below the value of 1.36 eV (see Table 1), except for E_D = 1.51 eV for the 'linear configuration' obtained with the H potential. This seemingly good agreement, however, should be taken with caution since the H potential overestimates the carbon migration energy by 0.45 eV. The value of 1.36 eV calculated with the J potential, should not be considered as reliable data either, because the C–C interaction is not included in the model. The R potential predicts E_D for a v–C_2 complex to be essentially lower than 1.5 eV. Analytical calculations performed by Tapasa et al. [31] show that the best fit to the experimental data obtained by Vehanen et al. [39], assuming that the stage at 490 K seen in [39] is the dissociation of v–C_2 complexes, is achieved by taking the binding energy between C and v–C equal to 0.8 eV. Calculations with the most reliable H potential give 0.17 and 0.12 eV for the linear and adjacent configurations, which is well below the expected number.

The dissociation energies of v_N–C complexes are also below 1.5 eV, except for $E_D(v_6–C)$ calculated with the R potential to be 1.54 eV (see Table 1). This number, however, should be considered as an overestimation (by ~0.4 eV) due to the incorrect description of v–C binding by the R potential (see discussion above). The only possible candidates (among the studied defects) for the dissociation stage occurring with the activation energy of 1.4 eV are v_3–C and v_4–C with E_D = 1.36 eV, obtained with the J potential. But the results obtained with the *a priori* more rigorous/reliable model (i.e. the H potential) do not confirm this. Hence, the performed calculations do not show that v–C_2 and v_N–C complexes have sufficiently high dissociation energy to explain the experimentally obtained recovery stage around 490 K. It can be speculated that higher order v_N–C_K clusters may be responsible for that stage, given that a weak attraction between carbon atoms located at a distance exceeding the second nearest neighbour shell is found with DFT [25].

5.2. Interaction of C with self-interstitial clusters

The strong attractive interaction between a ⟨1 1 0⟩ dumbbell and a carbon atom predicted by the J and R potentials [27] is inconsistent with the DFT results. The H potential accounts for the saturation of covalent bonding and thus is expected to provide a better description for the interaction of Carbon with over-coordinated defects. In the following discussion we shall put emphasis on the results obtained with the H potential. According to the latter, a carbon is not attracted to the small parallel and non-parallel clusters consisting of ⟨1 1 0⟩ dumbbells in the nearest neighbour coordination and hence should not affect the mobility of small 3D-migrating SIA clusters. RR experiments performed in Fe doped with carbon [19] did not reveal any effect of carbon on the migration of defects formed at stage I_E, i.e. di- and tri-SIA clusters. On the other hand it is known experimentally that carbon atoms are bound to dislocations and according to elasticity theory calculations the binding energy is 0.7 eV. Recent atomistic simulations performed using the J potential [23] have shown that a carbon atom exhibits a positive binding energy with both ½⟨1 1 1⟩ and ⟨1 0 0⟩ interstitial dislocation loops.

The results obtained for a 7-SIA cluster containing ⟨1 1 1⟩ crowdions suggest that all three potentials predict qualitatively and quantitatively similar behaviour for the interaction of C with the cluster. The maximum binding energy was found to be in the range 0.38–0.48 eV, which is rather strong but not high enough to explain the origin of the traps with the energy of ~1 eV (see introduction). A second carbon would offer a strong enough trapping but it should reach the cluster within the time required for the dissociation of C-cluster complex. Since the dissociation energy for the latter (0.4–0.6 eV) is much smaller than the migration energy of carbon in the bulk, multiple trapping can be excluded. Moreover, C–C interaction is known to be weak in Fe [24] so the concentration of C–C pairs should be negligibly small at elevated temperature. In irradiation conditions, most of carbon atoms in solution are expected to form stable complexes with vacancies (such as v–C and v–C_2), whose dissociation energy is at least above 1.0 eV. We therefore suggest that vacancy–carbon complexes can be responsible for the trapping of 1D migrating SIA clusters. MD simulations (see Section 4.2.2) show that the pinning strength of such complexes interacting with a ½⟨1 1 1⟩ interstitial loop is high enough to attribute the interaction energy of ~1 eV. We also note that the dissociation of v–C_2 (or v–C_N) complexes can occur due to the direct interaction with ⟨1 1 1⟩ SIA clusters, as was shown in the present work (see Section 4.2.2). In the latter case, relieved carbon atoms may diffuse around the loop core to occupy the trapping sites. The trapping energy estimated for the v–C complexes is also very close to the activation energy for the migration of nano-metric ½⟨1 1 1⟩ dislocation loops studied in ultra high pure Fe [13] and found to be 1.3 eV.

Finally, we recall that for the interaction of C with a straight ½⟨1 1 1⟩{1 1 0} edge dislocation and large ⟨1 1 1⟩ SIA cluster (61 SIA), the H potential gives qualitatively different results as compared to the two other potentials. The former model predicts an essential attractive interaction in the compressed region, whereas the two latter models point at a strong attractive interaction only in the tensile region. The clarification of the carbon properties in the vicinity of the dislocation core applying DFT calculations would be of high importance in assessing the validity of interatomic potentials. The energetics of carbon in the core of the edge dislocation was studied by electron delocalization molecular orbital theory calculations [41]. The Fe–C interaction was seen to be favoured in the dislocation region. It was found that the ½⟨1 1 1⟩{1 1 0} edge dislocation creates an energetically favourable zone for the accumulation of C, but no quantitative estimations of the binding energy and its dependence on the carbon position was provided. First principles calculations using the DMOL3 method have shown that C has a strong segregation tendency to enter the expansion region of the [0 0 1](1 0 0) dislocation core [42]. In both cases, the results of the above mentioned works are consistent with the considerations of the classical elasticity theory predicting the positive binding energy for C in the tensile region, i.e. consistent with the predictions of all the potentials used. However, it is only the H potential that predicts attractive interaction also for Carbon placed in the compressed region of the edge dislocation or dislocation loop, opposite to the J and R potentials and elasticity theory. In any case, elasticity theory considerations should be taken with caution, given that its accuracy is essentially questionable near the dislocation core region. The need for further DFT validation is clear. Yet, achievement of a reliable description of the edge dislocation core in a simulation cell containing a few hundreds of atoms is not a trivial task due to the strong hydrostatic pressure. Despite this, attempts to model edge dislocation were performed but nothing was reported about the size effect [42].

6. Conclusions

In this paper we report the study of the interaction of an interstitial carbon atom with SIA- and vacancy clusters in α-Fe. MS and MD simulations were performed using a combination of three different Fe–C interatomic potentials [25–27], including the most recent one, which accounts for the specific covalent bonding. The aim has been to investigate the impact of C on the stability and mobility of the small clusters of point defects. In addition, the interaction of 1-D migrating SIA clusters with immobile v–C_N ($N = 1, 2$) complexes was studied for the first time. The following conclusions can be drawn:

1. Earlier developed potentials [25,26] suggest that C stabilizes small vacancy clusters and reduces their mobility. Contrary to this, the metallic–covalent bonding potential [27] predicts that C exhibits attractive interaction only with vacancy clusters containing less than four vacancies.
2. None of the applied models is capable of reproducing correctly the binding energy of an additional carbon atom with a v–C pair, which was determined to be 0.8 eV according to DFT calculations [24]. The latter value was found to be sufficient to reproduce annealing experiments performed in C-doped α-Fe. The maximum binding energy found with the potentials used in this work was 0.5 eV. At this, the metallic–covalent bonding potential [27] predicts this value to be 0.17 eV. In addition, the metallic–covalent bonding potential was revealed to predict the path for an interstitial octahedral Carbon incorrectly and overestimate the actual migration energy by 0.45 eV, which is ∼50% of the value established by experiments and DFT calculations.
3. Static simulations performed using the metallic–covalent bonding potential did not reveal any considerable attractive interaction between C and small SIA clusters made of ⟨1 1 0⟩ dumbbells, contrary to the other two interatomic models. The former result is consistent with experimental RR studies reporting that defects migrating at stage II (i.e. di- and tri-SIA clusters) in C-doped Fe are not affected by carbon [19]. In addition, the metallic–covalent bonding potential does not show any essential attractive interaction between Carbon and small non-parallel SIA clusters [29]. Hence, Carbon does not stabilize them.
4. No drag of C by a ½⟨1 1 1⟩ SIA loop was revealed in dynamic simulations employing the metallic–covalent bonding potential, consistent with the early study done with the pairwise potential. As in the previous study [23], the change of a cluster's side was found to control the migration of a carbon in the core of a ½⟨1 1 1⟩ interstitial dislocation loop and hence to limit the C-loop drag process.
5. The weak attractive interaction of C with ½⟨1 1 1⟩ SIA clusters, found with the metallic–covalent bonding potential, is not sufficient to explain the origin of traps for 1D-glissle clusters, postulated in a number of kinetic Monte-Carlo studies dealing with the microstructural evolution of irradiated Fe [20,22]. Multiple carbon trapping is not expected to occur due to the short life time of a C-loop complex, unless the migrating loop encounters several carbon atoms instantaneously.
6. The interaction of a ½⟨1 1 1⟩ interstitial loop with both v–C and v–C_2 complexes was found to be much stronger than either with an isolated carbon atom or with a C–C pair. *Preliminary* estimates show that the stable and immobile v–C and v–C_2 complexes can indeed be responsible for the slowing down or complete blockage of ½⟨1 1 1⟩ SIA clusters, with a sufficiently high dissociation energy. Yet, additional static and dynamic simulations involving lower strain rates and/or higher temperature will help to make this conclusion more robust.

Acknowledgements

This work was supported by the European Commission (7th FWP, PERFORM60: 232612), the Spanish Ministry of Science and Innovation (FIS2009-13641-C02-02) and the Catalan Government (CIRIT 2009SGR 1003). The computing was partly made in CESCA (http://www.cesca.es). This work, was also carried out within the framework of the European Fusion Development Agreement.

References

[1] A. Foreman, W. Phythian, C. English, Philos. Mag. A 66 (1992) 671.
[2] R. Stoller, G. Odette, B. Wirth, J. Nucl. Mater. 251 (1997) 46.
[3] D. Bacon, F. Gao, Y. Osetsky, J. Nucl. Mater. 276 (2000) 1.
[4] D. Nguyen-Manh, S. Dudarev, A. Horsfield, J. Nucl. Mater. 367–370 (2007) 257.
[5] C. Domain, C. Becquart, Phys. Rev. B 65 (2002) 024103.
[6] F. Willaime, C. Fu, M. Marinica, J. Dalla Torre, Nucl. Instr. Methods Phys. Res. B 228 (2005) 92.
[7] Y. Osetsky, D. Bacon, A. Serra, B. Singh, S. Golubov, Phil. Mag. 83 (2003) 61.
[8] E. Kuramoto, K. Ohsawa, J. Imai, K. Obata, T. Tsutsumi, J. Nucl. Mater. 329–333 (2004) 1223.
[9] C. Fu, J. Dalla Torre, F. Willaime, J. Bocquet, A. Barbu, Nat. Mater. 4 (2005) 68.
[10] H. Trinkaus, B. Singh, A. Foreman, J. Nucl. Mater. 206 (1993) 200.
[11] B. Singh, S. Golubov, H. Trinkaus, A. Serra, Y. Osetsky, A. Barashev, J. Nucl. Mater. 251 (1997) 107.
[12] S. Golubov, B. Singh, H. Trinkaus, J. Nucl. Mater. 276 (2000) 78.
[13] K. Arakawa, K. Ono, M. Isshiki, K. Mimura, M. Uchikoshi, H. Mori, Science 318 (2007) 956.
[14] Y. Satoh, H. Matsui, T. Hamaoka, Phys. Rev. B 77 (2008) 094135.
[15] M.L. Jenkins, Z. Yao, M. Hernandez-Mayoral, M.A. Kirk, Dynamic observations of heavy-ion damage in Fe and Fe–Cr alloys, Symposium on Particle Beam Induced Radiation Effects in Materials held at the Annual Meeting of the Mineral-Metals-and-Materials-Society, New Orleans, LA, 2008, pp. 197.
[16] D. Terentyev, L. Malerba, M. Hou, Phys. Rev. B 74 (2007) 104108.
[17] N. Anento, A. Serra, Y.N. Osetsky, Modell. Simul. Mater. Sci. Eng. 18 (2010) 025008.
[18] S.L. Dudarev, M.R. Gilbert, K. Arakawa, H. Mori, Z. Yao, M.L. Jenkins, P.M. Derlet, Phys. Rev. B 81 (2010) 224107.
[19] S. Takaki, J. Fuss, H. Kugler, U. Dedek, H. Schultz, Radiat. Eff. 79 (1983) 87.
[20] C. Domain, C. Becquart, L. Malerba, J. Nucl. Mater. 335 (2004) 121.
[21] M. Caturla, N. Soneda, T. Diaz de la Rubia, M. Fluss, J. Nucl. Mater. 351 (2006) 78.
[22] M. Caturla, C. Ortiz, J. Nucl. Mater. 362 (2007) 141.
[23] K. Tapasa, A. Barashev, D. Bacon, Y. Osetsky, J. Nucl. Mater. 361 (2007) 52.
[24] C. Domain, C. Becquart, J. Foct, Phys. Rev. B 69 (2004) 144112.
[25] C. Becquart, J. Raulot, G. Bencteux, C. Domain, M. Perez, S. Garruchet, H. Nguyen, Comput. Mater. Sci. 40 (2007) 119.
[26] R. Johnson, Phys. Rev. 134 (1964) A1329.
[27] D. Hepburn, G. Ackland, Phys. Rev. B 78 (2008) 165115.
[28] Z. Rong, Y.N. Osetsky, D.J. Bacon, Phil. Mag. 85 (2005) 1473.
[29] D. Terentyev, T. Klaver, P. Olsson, M. Marinica, F. Willaime, C. Domain, L. Malerba, Phys. Rev. Lett. 100 (2008) 145503.
[30] E. Clouet, S. Garruchet, H. Nguyen, M. Perez, C. Becquart, Acta Mater. 56 (2008) 3450.
[31] K. Tapasa, A. Barashev, D. Bacon, Y. Osetsky, Acta Mater. 55 (2007) 1.
[32] K. Tapasa, Y.N. Osetsky, D.J. Bacon, Acta Mater. 55 (2007) 93.
[33] G. Ackland, M. Mendelev, D. Srolovitz, S. Han, A. Barashev, J. Phys.: Condens. Matter 16 (2004) 1.
[34] Y.N. Osetsky, D.J. Bacon, Modell. Simul. Mater. Sci. Eng. 11 (2003) 427.
[35] F. Willaime, J. Nucl. Mater. 323 (2003) 205.
[36] K. Tapasa, A.V. Barashev, D.J. Bacon, Y.N. Osetsky, J. Nucl. Mater. 361 (2007) 52.
[37] F. Djurabekova, L. Malerba, C. Domain, C. Becquart, Nucl. Instr. Methods Phys. Res. B 255 (2007) 47.
[38] W. Decker, J. Diehl, A. Dunlop, W. Frank, H. Kronmuller, W. Mensch, H.E. Schafer, B. Schewendemann, Phys. Status Solidi A 52 (1979) 239.
[39] A. VehanenP. Hautojärvi, J. Johansson, J. Yli-Kauppila, Phys. Rev. B 25 (1982) 762.
[40] A. Nikolaev, Phil. Mag. 87 (2007) 4847.
[41] S. Simonetti, M. Pronsato, G. Brizuela, A. Juan, Appl. Surf. Sci. 217 (2003) 56.
[42] J. Yan, C. Wang, W. Duan, S. Wang, Phys. Rev. B 69 (2004) 214110.